Published in final edited form as:
Biochem Pharmacol. 2011 October 15; 82(8): 852–861. doi:10.1016/j.bcp.2011.05.005.

Characterizing functional α6β2 nicotinic acetylcholine receptors *in vitro*: mutant β2 subunits improve membrane expression, and fluorescent proteins reveal responsive cells

Cheng Xiao[1,#], **Rahul Srinivasan**[1,#], **Ryan M. Drenan**[1], **Elisha D. W. Mackey**[1], **J. Michael McIntosh**[2], and **Henry A. Lester**[1,*]

[1]California Institute of Technology, Pasadena, CA, 91125, USA

[2]University of Utah, Salt Lake City, UT, 84112, USA

Abstract

α6* nicotinic acetylcholine receptors (nAChRs) are highly expressed in mesostriatal and nigrostriatal dopaminergic systems, and participate in motor control, reward, and learning and memory. *In vitro* functional expression of α6* nAChRs is essential for full pharmacological characterization of these receptors and for drug screening, but has been challenging. We expressed eGFP-tagged-α6 and β2 nAChR subunits in Neuro-2a cells, leading to functional channels. Inward currents were elicited with 300 μM ACh in 26% (5/19) of cells with evenly expressed α6-eGFP in cytoplasm and periphery. We dramatically increased chances of detecting functional α6-eGFPβ2 nAChRs by (i) introducing two endoplasmic reticulum (ER) export-enhancing mutations into β2 subunits, and (ii) choosing cells with abundant Sec24D-mCherry-labeled ER exit sites. Both manipulations also modestly increased α6-eGFPβ2 nAChR current amplitude. α6-eGFPβ2 nAChRs were also activated by nicotine and by TC-2403. The α6-eGFPβ2 currents were desensitized by 1 μM nicotine, blocked by α-conotoxin MII, partially inhibited by dihydro-β-erythroidine, and potentiated by extracellular Ca^{2+}. Single-channel recordings showed that α6-eGFPβ2 nAChRs had similar single channel conductance to, but longer open time than, α4-eGFPβ2 nAChRs. These methods provide avenues for developing cell lines expressing subtypes of α6* nAChRs for both pharmacological study and drug screening.

Keywords

nicotinic acetylcholine receptor; α6; β2; fluorescent protein; Neuro2a cell; endoplasmic reticulum exit sites

1. Introduction

Nicotinic acetylcholine receptors containing the α6-subunits (α6* nAChRs) are expressed in only a few mammalian brain regions [1–8], with high expression in mesolimbic and nigrostriatal dopaminergic systems. Current knowledge regarding α6* nAChR function and

*Corresponding author: Henry A. Lester 156-29 Caltech, Pasadena CA 91125 Phone: 626-395-4946; fax: 626-564-8709 lester@caltech.edu.
#These authors contributed equally to this study

drug screening is based primarily on mouse models, including lines lacking α6, α4, β2, or β3 subunits, as well as lines expressing hypersensitive α6 (L9′S) subunits [2–3, 5, 7–9]. α-conotoxin MII is an α6* nAChR antagonist[5–6]. Functional α6* nAChR responses can be isolated by measuring α-conotoxin MII-sensitive components of nicotine- or ACh- induced responses [2–3, 5, 9]. α6L9′S transgenic mice enable selective activation of α6* nAChRs with low concentrations of nicotine or other nicotinic ligands which activate α6* nAChRs [2–3].

These systems and protocols revealed that α6* nAChRs include a group of heteropentameric subtypes, including α6α4β2β3, α6α4β2, α6β2β3, and α6β2 nAChRs [2, 5, 7]. The β2 subunit is present in all characterized α6* nAChR combinations in dopaminergic neurons [8]. α6α4β3β2 nAChRs are the most sensitive subtype [7–8], and deleting either α4 or β3 subunits decreases receptor sensitivity [7]. α6* nAChRs participate in both motor control and reward. For instance, 1) Knocking out α4 subunits, which decreases the sensitivity of α6* nAChRs, eliminates behavioral hyperactivity observed in α6L9′S transgenic mice [2]; 2) α6* nAChRs are lost with degeneration of nigrostriatal dopaminergic system in Parkinson's disease [5–6, 10]; 3) Knocking out α6 subunits or blocking α6* nAChRs prevents nicotine self-administration [11–13]. Therefore, α6* nAChRs could be promising targets for both Parkinson's disease treatment and smoking cessation.

Progress in understanding α6* nAChR pharmacology is hindered by the fact that native expression systems currently available cannot adequately discriminate α6* nAChR subtypes. It is therefore important and necessary to establish robust and reproducible *In vitro* heterologous methods to express specific α6* nAChR combinations for pharmacological characterization and high-throughput drug screening.

Successful expression of functional α6* nAChRs in heterologous systems has so far been challenging [14–19]. In *In vitro* expression systems, α6 subunits form mature, functional receptors more efficiently with β4 subunits [15] than with β2 and β3 subunits [15–17, 19]. Although α6 and β2 subunits form agonist binding sites in human embryonic kidney cell lines, only 15% of cells show detectable ACh currents [20]. Kuryatov et al constructed chimeras replacing the extracellular domain of α3 or α4 subunit with that of α6 subunit, and also dimeric and trimeric concatamers. These constructs do form functional α6β2β3 nAChRs [17–18]; however, they could alter either the machinery of channel gating or high order structures of the receptors.

In this study, we fused enhanced green fluorescent protein (eGFP) within the intracellular M3–M4 loop of α6 subunits, and detected functional α6β2 nAChRs in 26% of Neuro-2a cells. Introducing a recently reported β2 subunit with enhanced endoplasmic reticulum (ER) export (β2-DM, also called $\beta2_{\text{enhanced-ER-export}}$) [21] dramatically increased the number of transfected cells expressing functional α6β2 nAChRs. Further, transfecting an mCherry-tagged ER exit site (ERES) marker (Sec24D-mCherry) facilitated visualizing and choosing cells expressing functional receptors. Studying this heterologous expression system, we characterized pharmacological and electrophysiological properties of α6β2 nAChRs with whole-cell and outside-out patch clamp recordings.

2. Methods and materials

2.1. Cell culture and nicotinic receptor transfection

α6-eGFP was subcloned from an α6-eYFP construct [14]. We transfected mouse α6-eGFPβ2-wt (wild type), α6-eGFPβ2-DM, or α4-eGFPα2-wt nAChRs into Neuro-2a cells (mouse neuroblastoma 2a, CCL-131). For transfections, sterilized 12 mm ø glass coverslips (Deckgläser, Czech Republic, Prague) were placed in 35-mm culture dishes. Fifty thousand

Neuro-2a cells in culture medium, composed of 45% DMEM, 45% Opti-MEM, 10% fetal bovine serum, were plated onto coverslips and cultured in an incubator (37°C, 95% air, 5% CO_2). Twenty four hours after plating, a mixture of 4 μl Expressfect Transfection Reagent (E2600, Denville Scientific Inc.) and appropriate plasmids were added to 0.2 ml DMEM, and equilibrated for 20 min at room temperature. Cells were washed with DMEM twice to remove culture medium, and incubated with 0.2 ml transfection mixture in 1 ml culture medium for 4 hours (37°C, 95% air, 5% CO_2). Cells were then washed twice with culture medium and incubated in a final volume of 3 ml culture medium. Forty-eight hours later, the cells were ready for electrophysiological recording or imaging. Plasmid concentrations for transfection were as follows: 500 ng α6-eGFP and 500 ng β2-wt / β2-DM subunits, with or without 250 ng Sec24D-mCherry. We previously reported the expression of other nAChRs and transporters with this expression system, with regard to dependence on DNA levels, trafficking, and surface density [21–23]. The sources of plasmids have been previously described [21].

2.2. Total Internal Reflection Fluorescent Microscopy (TIRFM)

Neuro-2a cells were cultured in glass-bottom poly-d-lysine-coated imaging dishes (MatTek Corporation, Ashland MA). Forty-eight hours after nAChR transfection, the culture dishes were transferred to a stage-mounted dish incubator (37°C) (Warner Instruments, Hamden CT) on an inverted microscope (IX71; Olympus). The microscope was equipped with an Olympus Plan Apo 100 × 1.45 numerical aperture oil objective and a Mitutoyo micrometer to control the position of the fiber optic and TIRF evanescent field illumination. TIRFM visualizes fluorescently labeled molecules within ~200 nm above the glass dish. Such molecules include those expressed in the cell membrane and in near-membrane intracellular structures [24–26]. eGFP fluorophores were excited with a 488-nm air-cooled argon laser, and an Optosplit II image splitter (Cairn Research, Faversham UK) was used to simultaneously detect fluorescence emission from eGFP and pCS2-mCherry, a plasma membrane (PM) marker.

Images were captured with an iXON DU-897, back-illuminated EM-CCD camera. Sample exposure rate, percent laser transmission, and gain parameters were initially adjusted, then maintained constant across all samples for each imaging session. 488-nm laser lines were linearly s-polarized as revealed using an achromatic 400 – 800-nm half-wave plate (AQWP05M-600; Thorlabs, Newton NJ).

The methodology for quantification of TIRFM images is described in detail elsewhere [21]. In brief, α6-eGFP served as a subcellular marker for nAChR localization. To obtain ER regions of interest (ROIs), average PM fluorescence intensity and background signal was subtracted from the entire TIRF image. PM fluorescence was extracted as follows: Raw TIRF images were converted to background-subtracted images and the ER fluorescence was thresholded and selected. ER fluorescence was then subtracted from the original image to generate images with PM fluorescence signals. These procedures yielded a dataset of several hundred thousand pixel intensities over 15 – 50 cells in each experimental group. Integrated densities are simply the sum of pixel values for either PM or ER or ER + PM (using whole TIRF footprint images). Mean pixel-based PM integrated densities were derived: dividing the total integrated density of all pixels of imaged cells from each experimental group by the number of imaged cells, and were used as pixel-based measure of the mean population of PM localized receptors. Ratios of integrated densities for whole TIRF footprint (ER + PM) to ER were used to determine the post-Golgi fraction of receptors. For PM integrated density measurements, rather than plotting SEMs (which would be indistinguishably small on the plots), we have used “error bars” to depict 99% confidence intervals based on a two-tailed *t* -test.

2.3. Spectral Confocal microscopy

A spectrally resolved laser-scanning confocal microscope (Eclipse C1si, Nikon) was equipped with a 63 × 1.4 numerical aperture VC Plan Apo oil objective. Before imaging, cell culture medium was replaced with phenol red-free CO_2-independent Leibovitz L-15 medium. All images were taken from live cells 48 h after transfection at 37°C. Cellular eGFP and mCherry fluorescence signals were acquired after sequential excitation with 488-nm (for eGFP) and 561-nm (for mCherry) lasers. Full-emission spectra were acquired in 5-nm bins between 500 and 660 nm, and the signal of each expressed fluorophore was linearly unmixed from the raw spectral image using reference spectra from control cells expressing only eGFP or only mCherry fusion constructs.

2.4. Patch clamp recordings

Recorded cells were visualized with an upright microscope (BX50WI; Olympus) in either bright field or fluorescence (eGFP and mCherry) mode. Electrophysiological signals were recorded with a MultiClamp 700B amplifier (Molecular Devices, Union City, CA), Digidata 1322 analog-to-digital converter (Axon Instruments), and pClamp 9.2 software (Axon Instruments). Patch pipettes were filled with solution containing (in mM): 135 K gluconate, 5 KCl, 5 EGTA, 0.5 $CaCl_2$, 10 HEPES, 2 Mg-ATP, and 0.1 GTP (pH was adjusted to 7.2 with Tris-base, and osmolarity was adjusted to 280 – 300 mOsm with sucrose). The resistance of patch pipettes was 4 – 6 MΩ for whole-cell recordings, and 12–15 MΩ for outside-out patch single-channel recordings. Junction potential was nulled just before forming a gigaseal. Series resistance was monitored without compensation throughout the experiment (Multiclamp 700B). The data were discarded if the series resistance (10 – 25 MΩ.) changed by more than 20% during recordings. All recordings were done at room temperature.

Data were sampled at 10 kHz and filtered at 2 kHz for whole-cell recordings, and sampled at 20 kHz and filtered at 4 kHz for single-channel recordings. Nicotinic agonists were dissolved in extracellular solution containing (in mM): 140 NaCl, 5 KCl, 2 $CaCl_2$, 1 $MgCl_2$, 10 HEPES, and 10 glucose (320 mOsm, pH set to 7.3 with Tris-base), and were puffed (0.1 or 3 s, 20 psi) onto voltage-clamped Neuro-2a cells (holding potential (V_H), −65 mV), or outside-out patches (V_H, −65 or −60 mV). To avoid receptor desensitization by repetitive ACh application, we applied ACh at ~3 min intervals, and continually perfused the recording chamber with extracellular solution [27–28].

2.5. Chemicals and applications

Mouse neuroblastoma 2a (Neuro-2a; CCL-131) cells were obtained from ATCC (Manassas, VA). pcDNA3.1(+) expression vectors and fetal bovine serum were purchased from Invitrogen (Carlsbad, CA). Expressfect was purchased from Denville Scientific (South Plainfield, NJ). Acetylcholine chloride (ACh), dihydro-β-erythroidine hydrobromide (DHβE), and (−)-nicotine hydrogen tartrate salt (nicotine) were from Sigma-Aldrich (St. Louis, MO). TC-2403 was provided by Targacept Inc. (Winston-Salem, NC).

2.6. Data analysis

Clampfit 9.2 was used to analyze both whole-cell and single-channel currents. For whole-cell currents, we low-pass filtered traces at 1 kHz, measured peak amplitude, and estimated decay time constant by fitting 10 – 90% of decay with one or two exponential terms. A Chi-square test was used to compare incidences of α6β2 nAChR current among cells with different transfections (α6-eGFPβ2-wt, α6-eGFPβ2-DM, and α6-eGFPβ2-DM plus Sec24D-mCherry). The difference of decay time constant between groups of cells was assayed by one-way ANOVA. When drug effects were tested, the amplitude of ACh-induced currents

during the application of antagonists or 1 μM nicotine was normalized to its mean value observed during control period (average of 3 responses). Drug effects were expressed as % inhibition (mean ± SEM), while the recovery after drug washout was expressed as % of control values. The statistical significance of drug effects was assessed by a paired two-tailed t-test.

In outside-out patch recordings, we selected single-channel events that occurred within 5 s after ACh puffs (Fig. $6A_1$, B_1). This time window matches the decay of whole-cell currents (Fig. 1, 4). We low-pass filtered signals at 4 kHz by Gaussian or Butterworth-8-pole filters, and used the event detection feature (single-channel search) in Clampfit to detect channel openings that were longer than 0.1 ms (Fig. $6A_2$, B_2). We pooled all events from cells transfected with either α6-GFPβ2-DM or α4-GFPβ2 nAChRs, and plotted histograms for both amplitude (0.1 pA per bin) and dwell time (0.2 ms per bin) of one-level openings (Fig. 6). The mean of each parameter was estimated after curve fitting. The amplitude distribution was fitted by a Gaussian relation, and the distribution of open times was fitted to a single exponential relation. We performed a two-tailed t-test to compare single-channel conductance, and used the Kolmogorov-Smirnov test to compare open time between α6-GFPβ2-DM and α4-GFPβ2-wt nAChRs.

Values of $p < 0.05$ were considered significant.

3. Results

3.1. ACh-induced currents in Neuro-2a cells transfected with α6-eGFPβ2-wt and α4-eGFPβ2-wt nAChRs

In order to visualize α6β2 nAChRs, we transfected Neuro-2a cells with α6-eGFP and β2-wt nAChR subunits. Forty-eight hours after transfection, most eGFP-positive cells showed cytoplasmic localization of eGFP aggregates. In a small fraction of cells, eGFP was evenly expressed in cytoplasm and periphery (Fig. 3A). Since peripheral receptors may include those inserted in PM, which could respond to agonist, we selected cells that evenly expressed –6-eGFP in cytoplasm and periphery (Fig. 3 A) for patch clamp recording. We recorded inward currents in 26% (5 / 19) of cells in response to puffed ACh (300 μM, 0.1 s, 20 psi) (Fig. $1A_1$). Using the same methods, we transfected α4-eGFP plus β2-wt subunits into Neuro-2a cells [21]. Forty-eight hours after transfection, we detected ACh-induced inward currents from all recorded α4-eGFP-positive cells (Fig. $1A_{2–3}$).

300 μM ACh-induced inward currents in α6-eGFPβ2-wt cells (54 ± 10 pA, n = 5, Fig. $1A_1$, B) were much smaller than those in α4-eGFPβ2-wt cells (690 ± 140 pA, n = 9, Fig. $1A_3$, B). Although 3 μM ACh induced no current in α6-eGFPβ2-wt cells that responded to 300 μM ACh (n = 2, data not shown), it evoked inward currents (73 ± 12 pA, n = 9, Fig. $1A_2$, B) in cells transfected with α4-eGFPβ2-wt nAChRs. The averaged decay time constant of 300 μM ACh-induced α6-eGFPβ2-wt currents was 333 ± 67 ms (n = 5), while that of 3 and 300 μM ACh-induced α4-eGFPβ2-wt currents was respectively 932 ± 69 ms (n = 9) and 1686 ± 120 ms (n = 9) (Fig. 1C).

All known nAChRs are at least 50% activated by 300 μM ACh used in the experiment of Fig. 1 [29–30]. α6β2 nAChRs are not exceptional in this regard [20]. Therefore, it is unlikely that the small size of the observed ACh-induced α6-eGFPβ2-wt currents arose from the activation of a small fraction of functional receptors, although we have not gathered systematic dose-response data. It seemed more appropriate to pursue the hypothesis that a large majority of α6-eGFPβ2-wt nAChRs do not insert into the PM. This supposition motivated the experiments described below.

3.2. β2 subunits with enhanced ER export mutations increased membrane insertion of α6-eGFPβ2 nAChRs

The mouse β2 subunit has an ER retention / retrieval motif (365RRQR368), but lacks an ER export motif (347LFL349, instead of 347LFM349) [21]. We previously measured the effects of disrupting the ER retention motif (365AAQA368) and reconstituting ER export motif (347LFM349) in the β2 subunit; the doubly mutant β2 subunit is called β2-DM or $\beta2_{\text{enhanced-ER-export}}$. Incorporation of α2-DM increases the number of ERES [21] and subsequently facilitates PM insertion of α4-eGFPβ2 nAChRs. We were encouraged to conduct analogous experiments with α6 subunits, because the β4 subunit possesses an ER export motif and lacks an ER retention / retrieval motif [21]; and both α4β4 and α6β4 nAChRs show much more functional expression than the corresponding α4β2 and α6β2 heteropentamers [15, 21]. Therefore, we hypothesized that these mutants could enhance membrane insertion of α6-eGFPβ2 nAChRs.

TIRF microscopy enables visualization of fluorophores within ~200 nm of PM [24–26]. Our studies showed that TIRFM detects fluorescent protein-tagged nAChRs localized in the PM and peripheral ER [14, 21]. In TIRF footprints, ER is characterized by reticulate labeling, while PM shows uniform fluorescence. Subcellular differences in fluorescence labeling became apparent in PM and ER subtracted TIRF images (Fig. 2A). We consistently observed that ER was 2 to 3 folds brighter than PM. We exploited subcellular differences in morphology and fluorescence intensity to separately demarcate and quantify PM and ER fluorescence (Fig. 2A, see Methods).

To confirm our hypotheses, we used TIRFM to compare PM localization of α6-eGFPβ2-wt and α6-eGFPβ2-DM nAChRs. The average pixel-based measure of PM integrated density for α6-eGFPβ2-DM receptors was ~2 folds greater than that of α6-eGFPβ2-wt nAChRs (Fig. 2B). We utilized ratios of whole cell footprint to ER integrated density to quantify ER-associated changes in receptor localization. The ratio for α6-eGFPβ2-DM nAChRs (~1.2) was only slightly higher than that for α6-eGFPβ2-wt nAChRs in Neuro-2a cells (Fig. 2C), while it is substantially lower than the corresponding parameter for α4β2 nAChRs (3 – 4) and α4β2-DM nAChRs (7 – 9) [21].

To enhance our chances of detecting functional α6-eGFPβ2 nAChRs, we performed electrophysiological recordings in Neuro-2a cells transiently expressing α6-eGFPβ2-DM nAChRs. As expected, 300 μM ACh evoked inward currents in a significantly larger proportion of α6-eGFPβ2-DM cells (28 out of 51) than in α6-eGFPβ2-wt cells (5 out of 19) ($p = 0.03$) (Fig. 3C).

These results only partially confirm the hypothesis that the β2-DM subunits could enhance ER export and, eventually, PM insertion of α6-eGFPβ2 nAChRs. Most α6β2-DM nAChRs remained trapped in the ER, although the ER exit rate was apparently great enough to produce an increased fraction of cells with functional PM nAChRs.

3.3. Visualization of a fluorescently tagged ERES marker

We continued to pursue the hypothesis that ER trapping dominates the poor surface expression of α6β2 nAChRs. We transfected Neuro-2a cells with α6-eGFPβ2-DM, and Sec24D-mCherry, a fluorescently-tagged ERES marker, as well. When we chose cells with moderate to high density of α6-eGFP (Fig. $3B_1$), and abundant, large and bright ERES (Fig. $3B_2$), we detected inward currents (300 μM ACh) in 86% (24 / 28) of cells (Fig. 3C). Therefore, choosing cells with more ERES dramatically increased our chances of detecting functional α6-eGFPβ2-DM nAChRs. The rather small number of cells displaying α6-eGFPβ2-wt nAChR currents vitiated systematic study of these responses. However Fig. 3D conveys the impression that, compared with α6-eGFPβ2-wt nAChR currents, the distribution

of α6-eGFPβ2-DM nAChR currents in cells co-transfected with or without Sec24D-mCherry was similar at the two lower quartiles (<50%), but larger at the highest quartile (> 75%). The average responses for the three groups were similar within 25% (α6-eGFPβ2-DM: 70 ± 11 pA, n = 28; α6-eGFPβ2-DM plus Sec24D-mCherry: 66 ± 10 pA, n = 24; α6-eGFPβ2-wt: 54 ± 10 pA, n = 5). The increased incidence of α6-eGFPβ2 nAChR currents suggested that introducing β2-DM increased membrane insertion of α6-eGFPβ2 nAChRs, while the ERES marker could facilitate choosing cells expressing functional receptors. We do not know whether the effects of the fluorescent Sec24D arise solely from our ability to visualize cells with increased ERES, or also from the increased COPII levels in those cells.

Lack of difference in response waveforms among α6-eGFPβ2-wt, α6-eGFPβ2-DM, and α6-eGFPβ2-DM plus Sec24D-mCherry cells (Fig. 3E) suggested that neither β2-DM nor Sec24D-mCherry altered the intrinsic functional properties of α6β2 nAChRs. The observations gave us the confidence to conduct electrophysiological and pharmacological studies of the expressed α6β2 nAChRs.

3.4. Pharmacological properties of heterologously expressed α6β2 nAChRs in Neuro-2a cells

We observed that both nicotine and TC-2403 activated inward currents in cells expressing functional α6-eGFPβ2-DM nAChRs (Fig. 4A, B). This is consistent with a previous study showing that nicotine and TC-2403 stimulate both dopamine release and locomotion in α6L9'S transgenic mice [3].

Next we tested whether functional α6-eGFPβ2-wt / α6-eGFPβ2-DM nAChRs could be blocked by either α6* or β2* nAChR antagonists. In this set of experiments, antagonists were added in the perfusate at the intended concentration, until stable effects were obtained. Indeed, the α6β2 currents were blocked by 80 nM α-conotoxin MII, an antagonist of α3* and α6* nAChRs (Fig. $4C_{1–2}$). The currents recovered to 70 ± 8% (n = 5, $p = 0.01$) of initial values after 20 min washout. DHβE (300 nM), a selective antagonist for β2* nAChRs, blocked 300 μM ACh-induced α4-eGFPβ2 nAChR currents (by 97 ± 1%, n = 3, $p = 0.00001$, data not shown), and the currents recovered to about 50% of baseline values after 15 min washout (data not shown). However, α6-eGFPβ2-DM nAChRs showed lower sensitivity to DHβE, along with faster and greater recovery (Fig. $4D_{1–2}$). In particular, 300 nM and 2 μM DHβE inhibited α6-eGFPβ2-DM nAChR currents by 39 ± 3% (n = 4, $p = 0.0005$) and 59 ± 9% (n = 4, $p = 0.003$), respectively, while the currents recovered to 90 ± 5% (n = 5) of initial currents following 10 min washout of 2 μM DHβE. These data suggest that α6β2 nAChRs might have lower affinity to DHβE than α4β2 nAChRs.

We found that removing extracellular Ca^{2+} by replacing 2 mM Ca^{2+} with 2 mM Mg^{2+} (0 Ca^{2+}) significantly decreased α4-eGFPβ2-wt nAChR currents by 30 ± 7% (n = 4, $p = 0.008$, Fig. $4E_2$). A similar phenomenon was observed in α6-eGFPβ2-DM nAChRs (Fig. $4E_1$). In 0 Ca^{2+} medium, 300 μM ACh-induced currents diminished by 30 ± 3% (n = 4, $p = 0.00004$, Fig. $4E_2$). These data on Ca^{2+} modulation of α6β2 nAChRs resemble results with other nAChR subunit combinations [31–32].

3.5. Desensitization of α6-eGFPβ2-DM nAChRs

Desensitization is a common property of nAChRs. The ACh puffs (0.1 s) used to evoke α6-eGFPβ2-DM nAChR currents were one order of magnitude briefer than the decay time constant of the currents (Fig. 1, Fig. 4). The current decay could be a consequence of either agonist diffusion, deactivation of receptors due to agonist dissociation, receptor desensitization, or a combination of these processes. To isolate the role of desensitization in response waveforms, we puffed 300 μM ACh for 3 s (Fig. $5A_1$). The α6-eGFPβ2-DM

nAChR current decay was described successfully by a two-exponential function (see in Methods). The faster (τ = 283 ± 24 ms, n = 7) and slower component (τ = 3528 ± 349 ms, n = 7) respectively account for 66 ± 5% (n = 7) and 23 ± 4% (n = 7) of peak amplitude.

Next we examined α6-eGFPβ2-DM nAChR desensitization by 1μM nicotine. We puffed 300 μM ACh (0.1 s) onto Neuro-2a cells to induce α6-eGFPβ2-DM nAChR currents at 3 min intervals. After a stable baseline response was established (~10 min), we added 1 μM nicotine into the perfusate, and found that ACh-induced currents diminished to nearly zero within a few min (Fig. $5B_{1-2}$). The currents recovered to 58 ± 3% of initial values (n = 3) after 6 min washout, and reached 88 ± 2% (n = 3) of initial values after 20 min washout.

3.6. Single-channel analysis of α6β2 and α4β2 nAChR currents in Neuro-2a cells

To characterize the function of α6β2 nAChRs at the single-channel level, and to compare with α4β2 nAChR function, we performed outside-out patch single-channel recordings from cells that displayed 300 μM ACh-induced inward currents in whole-cell mode. As illustrated in Fig. $6A_1$, 300 μM ACh (0.1 s)-induced events show 1 – 2 opening levels in voltage-clamped patches (VH, −60 mV) from the cells transfected with α6-eGFPβ2-DM nAChRs. However, 300 μM ACh evoked 20 – 40 pA currents in voltage-clamped patches (V_H, − 65 mV) from the cells transfected with α4-eGFPβ2 nAChRs (data not shown). We decreased ACh concentration to 3 μM to limit the number of α4-eGFPβ2 nAChRs being activated. This strategy provided us with unambiguous single-channel events for further analysis. As illustrated in Fig. $6B_1$, 3 μM ACh evoked ≤ 3 levels of channel openings. In both α6-eGFPβ2-DM and α4-eGFPβ2 patches, we observed that ACh produced channel opening over a time course of ~5 s, (Fig. $6A_1$, B_1), similar to the waveform of whole-cell responses to ACh puffs (Fig. 1, 4). Fig. $6A_2$ and B_2 show expanded traces of single level openings. We pooled single level opening events from 10 α6-eGFPβ2-DM patches and 7 α4-eGFPβ2-wt patches. The single-channel conductance of α6-eGFPβ2-DM nAChRs (24 pS) was similar to that of α4-eGFPβ2-wt nAChRs (26.2 pS) (p = 0.35, two tailed t-test) (Fig. $6A_3$, B_3). The single-channel open time of α6-eGFPβ2-DM nAChRs (τ = 1.4 ms, n = 279) was significantly longer than that of α4-eGFPβ2-wt nAChRs (τ = 0.6 ms, n = 875) ($p < 0.0001$, Kolmogorov-Smirnov test) (Fig. $6A_4$, B_4).

4. Discussion

4.1. Increasing the membrane expression of α6β2 nAChRs by enhancing ER export

After transfecting Neuro-2a cells with α6-eGFPβ2 nAChRs, we selected cells with uniform expression of α6-eGFP in cytoplasm and periphery (Fig. 3A), presumably indicating surface expression. This provided a modest success rate (26%, Fig. $1A_1$, 3C), higher than previous studies [14, 18, 20], which showed zero to 15%. When we replaced β2-wt with β2-DM subunits, we observed 1) that PM insertion of α6-eGFP was increased by 2 fold (Fig. 2B), 2) that functional α6β2 nAChRs were detected in more than half of transfected cells (Fig. 3C), and 3) that ACh induced larger currents in some transfected cells (Fig. 3D).

To achieve even greater success rates, we also fluorescently tagged Sec24D molecules. Following assembly, nAChRs bind to Sec24D through LFM motifs in M3-M4 loop, resulting in the formation of specialized ERES [21, 33–34]. ERES number increases in direct proportion to nAChR export rate [21]. Therefore, cells having more ERES could more efficiently export nAChRs to PM. Indeed, 86% of cells with abundant, bright, and large ERES (Fig. $3B_2$), displayed functional α6-eGFPβ2-DM nAChRs (Fig. 3C). Although current amplitude in the selected cells was modestly (22%) larger than that in cells transfected with α6-eGFPβ2-wt nAChRs, it was similar to that in cells transfected with α6-eGFPβ2-DM nAChRs (Fig. 3D). Apparently ACh responses occur in α6-eGFPβ2-DM cells

with abundant and large ERES; and the ERES marker enabled the visualization of α6-eGFPβ2-DM cells expressing functional receptors.

4.2. Pharmacology of α6β2 nAChRs

In this study, α6β2 nAChRs were activated by ACh, nicotine (Fig. 4A), and TC-2403 (Fig. 4B), consistent with a previous study using α6L9'S transgenic mice [3], although another study found that TC-2403 has no detectable agonist activity at α6β2* nAChRs [9]. The α6-eGFPβ2-DM nAChRs were blocked by α-conotoxin MII, recovering after 20 min washout (Fig. $4C_{1–2}$). This recovery is not directly comparable with the slower recovery shown in previous studies using native systems, including brain slices and synaptosomes [3, 8, 28]. It is possible that α6* nAChR subtypes (e.g. those containing β3 and/or α4 subunits) could have different dissociation rates for α-conotoxin MII. Interestingly, α6β2 nAChRs were partially and reversibly blocked by DHβE (Fig. $4D_{1–2}$), contrasting with the fact that α4β2 nAChRs are blocked by DHβE at low hundreds nM.

We also observed that at levels achieved during smoking, nicotine desensitized α6β2 nAChRs (Fig. $5B_{1–2}$). The effect is roughly as robust as previous studies on α4β2 nAChRs [35–36]. However, when nicotine was washed out, α6β2 nAChR currents recovered more rapidly and thoroughly than α4β2 nAChR currents [35]. These data suggested 1) that the desensitized state(s) of α6β2 nAChRs might have lower affinity to nicotine than α4β2 nAChRs; 2) that α6β2 nAChRs would regain function more readily than α4β2 nAChRs if desensitized.

Extracellular Ca^{2+} allosterically modulates nAChRs, and increases channel opening probability [31–32]. In the brain, high levels of neuronal activity deplete extracellular Ca^{2+}, and this could lower opening probability of nAChRs [37–38]. We observed that removal of extracellular Ca^{2+} decreased both α4β2 and α6β2 nAChR currents to roughly the same extent (Fig. 4E), suggesting that α6β2 nAChRs could also be modulated by neuronal activity *in vivo*.

Our pharmacological data thus indicate that α6β2 nAChRs could be distinguished from α4β2 nAChRs by their resistance to DHβE and rapid recovery from nicotine desensitization. In some situations, desensitization could be physiologically relevant by changing the balance of excitation and inhibition in neural circuits [39–40].

4.3. Electrophysiological characterization of α6β2 nAChRs

We observed that the decay of α6-eGFPβ2-DM nAChR currents, evoked by 3 s puff of 300 μM ACh, was described by a two-exponential function (Fig. $5A_{1–2}$). This suggested either that multiple processes account for "desensitization" of individual α6β2 nAChRs, or that more than one population of α6β2 nAChRs exist, with different desensitization rates (Fig. $5A_2$). By analogy with α4β2 nAChRs (see next paragraph), it would not be surprising to find that these two components could reflect different receptor stoichiometries: $(\alpha6)_3(\beta2)_2$ and $(\alpha6)_2(\beta2)_3$. Further investigations would test this hypothesis by performing 1) Förster resonance energy transfer [21–22], 2) biased transfections of α6 and β2 subunits with different ratios to assess changes in the predominance of faster and slower components [41–42], and 3) systematic dose-response studies [41–43]. Additionally, the physiological significance of these two components also warrants further investigations.

α4β2 nAChRs assemble into two stoichiometries: $(\alpha4)_3(\beta2)_2$ and $(\alpha4)_2(\beta2)_3$ [21–22, 41–44]. Low concentrations (< 10 μM) of ACh primarily activate high sensitivity α4β2 nAChRs, while high concentrations (≥ 100 μM) of ACh activate both. Previous studies revealed that high sensitivity α4β2 nAChRs have smaller single-channel conductance (17 – 31 pS) than low sensitivity receptors (44 – 46 pS) [32, 43–48]. In this study, we activated α4β2 nAChRs

on voltage-clamped outside-out patches by 3 μM ACh (Fig. $6B_1$). Given this concentration and the single-channel conductance of 26.2 pS (Fig. $6B_2$), we suggest that most of the α4β2 single-channel events were mediated by high sensitivity receptors.

A previous study reported that the EC_{50} of ACh for α6β2 nAChRs is 150 μM [20]. Therefore, 300 μM ACh can activate both high and low sensitivity α6β2 nAChRs if any. We observed a single conductance component in 300 μM ACh-induced single α6β2 nAChR currents (Fig. $6A_{2–3}$). It could be 1) that, in our transfection condition, the majority of α6β2 nAChRs assembled in one stoichiometry, and the number of recorded events were too low to show a minority component, or 2) that α6β2 nAChRs in two stoichiometries could have the same single-channel conductance or even a single sensitivity component as previously reported [20]. The average conductance of α6β2 nAChRs was 24 pS, which was similar to that of α4β2 nAChRs (26.2 pS) (Fig. $6A_3$, B_3). The single-channel duration of α6β2 nAChRs was significantly longer than that of α4β2 nAChRs. We applied 3 μM ACh to activate α4β2 nAChR single-channel events, but applied 300 μM ACh to activate α6β2 nAChR single channel events, and still observed that α4β2 nAChRs opened more frequently (875 events / 25.3 s) than α6β2 nAChRs (279 events / 50 s). The low open probability of α6β2 nAChRs could result from the high concentration of ACh, which could cause receptor desensitization.

4.4. Additional subunits and stoichiometries?

Note that native α6* nAChRs include several subunit combinations and stoichiometries. The α6β2 nAChRs studied here may be the subtype with the least sensitivity to agonists, the lowest binding affinity to α-conotoxin MII and DHβE, and the least biological relevance. The α6α4β2* nAChRs could be the major physiologically relevant subtypes for dopamine release [2]. Including α4 and/or β3 subunits in α6β2* nAChRs increases receptor sensitivity [7–8], and including β3 subunits also increases expression levels [15–17, 19].

Thus we can hope that the present techniques for expressing purely α6β2 nAChRs (β2-DM subunits, fluorescently tagged α6 subunits, and ERES markers) may have overcome the greatest hurdle. However, we do not yet know whether one or more of the strategies introduced here could also increase chances of detecting functional α4α6β2 and α4α6β2β3 nAChRs in Neuro-2a cells. If so, these systems could be used to investigate pharmacological and electrophysiological properties of α6* nAChRs subtypes, and may facilitate drug screening for both Parkinson's disease protection and smoking cessation.

Acknowledgments

This work was supported by grants from the US National Institutes of Health (DA17279, NS11756, AG033954, DA19375, DA12242, MH53631, and GM48677); from Targacept Inc.; from the California Tobacco-Related Disease Research Program (TRDRP); and from Louis and Janet Fletcher. R. S. was supported by a postdoctoral fellowship from TRDRP (18FT-0066), and R. D. by an NIH National Research Service Award (DA021492) and an NIH Pathway to Independence Award (DA030396).

5. References

[1]. Calabresi P, Di Filippo M. ACh/dopamine crosstalk in motor control and reward: a crucial role for α6-containing nicotinic receptors? Neuron. 2008; 60:4–7. [PubMed: 18940582]

[2]. Drenan RM, Grady SR, Steele AD, McKinney S, Patzlaff NE, McIntosh JM, et al. Cholinergic modulation of locomotion and striatal dopamine release is mediated by α6α4* nicotinic acetylcholine receptors. J Neurosci. 2010; 30:9877–89. [PubMed: 20660270]

[3]. Drenan RM, Grady SR, Whiteaker P, McClure-Begley T, McKinney S, Miwa JM, et al. In vivo activation of midbrain dopamine neurons via sensitized, high-affinity α6 nicotinic acetylcholine receptors. Neuron. 2008; 60:123–36. [PubMed: 18940593]

[4]. Gaimarri A, Moretti M, Riganti L, Zanardi A, Clementi F, Gotti C. Regulation of neuronal nicotinic receptor traffic and expression. Brain Res Rev. 2007; 55:134–43. [PubMed: 17383007]

[5]. Grady SR, Salminen O, Laverty DC, Whiteaker P, McIntosh JM, Collins AC, et al. The subtypes of nicotinic acetylcholine receptors on dopaminergic terminals of mouse striatum. Biochem Pharmacol. 2007; 74:1235–46. [PubMed: 17825262]

[6]. Quik M, McIntosh JM. Striatal α6* nicotinic acetylcholine receptors: potential targets for Parkinson's disease therapy. J Pharmacol Exp Ther. 2006; 316:481–9. [PubMed: 16210393]

[7]. Salminen O, Drapeau JA, McIntosh JM, Collins AC, Marks MJ, Grady SR. Pharmacology of α-conotoxin MII-sensitive subtypes of nicotinic acetylcholine receptors isolated by breeding of null mutant mice. Mol Pharmacol. 2007; 71:1563–71. [PubMed: 17341654]

[8]. Salminen O, Murphy KL, McIntosh JM, Drago J, Marks MJ, Collins AC, et al. Subunit composition and pharmacology of two classes of striatal presynaptic nicotinic acetylcholine receptors mediating dopamine release in mice. Mol Pharmacol. 2004; 65:1526–35. [PubMed: 15155845]

[9]. Grady SR, Drenan RM, Breining SR, Yohannes D, Wageman CR, Fedorov NB, et al. Structural differences determine the relative selectivity of nicotinic compounds for native α4β2*-, α6β2*-, α3β4*- and α7-nicotine acetylcholine receptors. Neuropharmacology. 2010; 58:1054–66. [PubMed: 20114055]

[10]. Perez XA, Bordia T, McIntosh JM, Grady SR, Quik M. Long-term nicotine treatment differentially regulates striatal α6α4β2* and α6(nonα4)β2* nAChR expression and function. Mol Pharmacol. 2008; 74:844–53. [PubMed: 18583454]

[11]. Brunzell DH, Boschen KE, Hendrick ES, Beardsley PM, McIntosh JM. α-conotoxin MII-sensitive nicotinic acetylcholine receptors in the nucleus accumbens shell regulate progressive ratio responding maintained by nicotine. Neuropsychopharmacology. 2010; 35:665–73. [PubMed: 19890263]

[12]. Jackson KJ, McIntosh JM, Brunzell DH, Sanjakdar SS, Damaj MI. The role of α6-containing nicotinic acetylcholine receptors in nicotine reward and withdrawal. J Pharmacol Exp Ther. 2009; 331:547–54. [PubMed: 19644040]

[13]. Pons S, Fattore L, Cossu G, Tolu S, Porcu E, McIntosh JM, et al. Crucial role of α4 and α6 nicotinic acetylcholine receptor subunits from ventral tegmental area in systemic nicotine self-administration. J Neurosci. 2008; 28:12318–27. [PubMed: 19020025]

[14]. Drenan RM, Nashmi R, Imoukhuede P, Just H, McKinney S, Lester HA. Subcellular trafficking, pentameric assembly, and subunit stoichiometry of neuronal nicotinic acetylcholine receptors containing fluorescently labeled α6 and β3 subunits. Mol Pharmacol. 2008; 73:27–41. [PubMed: 17932221]

[15]. Gerzanich V, Kuryatov A, Anand R, Lindstrom J. "Orphan" α6 nicotinic AChR subunit can form a functional heteromeric acetylcholine receptor. Mol Pharmacol. 1997; 51:320–7. [PubMed: 9203638]

[16]. Grinevich VP, Letchworth SR, Lindenberger KA, Menager J, Mary V, Sadieva KA, et al. Heterologous expression of human α6β4β3α5 nicotinic acetylcholine receptors: binding properties consistent with their natural expression require quaternary subunit assembly including the α5 subunit. J Pharmacol Exp Ther. 2005; 312:619–26. [PubMed: 15356217]

[17]. Kuryatov A, Lindstrom J. Expression of functional human α6β2β3* acetylcholine receptors in Xenopus laevis oocytes achieved through subunit chimeras and concatamers. Mol Pharmacol. 2011; 79:126–40. [PubMed: 20923852]

[18]. Kuryatov A, Olale F, Cooper J, Choi C, Lindstrom J. Human α6 AChR subtypes: subunit composition, assembly, and pharmacological responses. Neuropharmacology. 2000; 39:2570–90. [PubMed: 11044728]

[19]. Tumkosit P, Kuryatov A, Luo J, Lindstrom J. β3 subunits promote expression and nicotine-induced up-regulation of human nicotinic α6* nicotinic acetylcholine receptors expressed in transfected cell lines. Mol Pharmacol. 2006; 70:1358–68. [PubMed: 16835356]

[20]. Walsh H, Govind AP, Mastro R, Hoda JC, Bertrand D, Vallejo Y, et al. Up-regulation of nicotinic receptors by nicotine varies with receptor subtype. J Biol Chem. 2008; 283:6022–32. [PubMed: 18174175]

[21]. Srinivasan R, Pantoja R, Moss FJ, Mackey ED, Son CD, Miwa J, et al. Nicotine up-regulates α4β2 nicotinic receptors and ER exit sites via stoichiometry-dependent chaperoning. J Gen Physiol. 2011; 137:59–79. [PubMed: 21187334]

[22]. Son CD, Moss FJ, Cohen BN, Lester HA. Nicotine normalizes intracellular subunit stoichiometry of nicotinic receptors carrying mutations linked to autosomal dominant nocturnal frontal lobe epilepsy. Mol Pharmacol. 2009; 75:1137–48. [PubMed: 19237585]

[23]. Imoukhuede PI, Moss FJ, Michael DJ, Chow RH, Lester HA. Ezrin mediates tethering of the γ-aminobutyric acid transporter GAT1 to actin filaments via a C-terminal PDZ-interacting domain. Biophys J. 2009; 96:2949–60. [PubMed: 19348776]

[24]. Fish KN. Total internal reflection fluorescence (TIRF) microscopy. Curr Protoc Cytom. 2009:8. Chapter 12:Unit12.

[25]. Khiroug SS, Pryazhnikov E, Coleman SK, Jeromin A, Keinanen K, Khiroug L. Dynamic visualization of membrane-inserted fraction of pHluorin-tagged channels using repetitive acidification technique. BMC Neurosci. 2009; 10:141. [PubMed: 19948025]

[26]. Oancea E, Wolfe JT, Clapham DE. Functional TRPM7 channels accumulate at the plasma membrane in response to fluid flow. Circ Res. 2006; 98:245–53. [PubMed: 16357306]

[27]. Tapper AR, McKinney SL, Nashmi R, Schwarz J, Deshpande P, Labarca C, et al. Nicotine activation of α4* receptors: sufficient for reward, tolerance, and sensitization. Science. 2004; 306:1029–32. [PubMed: 15528443]

[28]. Xiao C, Nashmi R, McKinney S, Cai H, McIntosh JM, Lester HA. Chronic nicotine selectively enhances α4β2* nicotinic acetylcholine receptors in the nigrostriatal dopamine pathway. J Neurosci. 2009; 29:12428–39. [PubMed: 19812319]

[29]. Chavez-Noriega LE, Crona JH, Washburn MS, Urrutia A, Elliott KJ, Johnson EC. Pharmacological characterization of recombinant human neuronal nicotinic acetylcholine receptors hα2β2, hα2β4, hα3β2, hα3β4, hα4β2, hα4β4 and hα7 expressed in Xenopus oocytes. J Pharmacol Exp Ther. 1997; 280:346–56. [PubMed: 8996215]

[30]. Gerzanich V, Peng X, Wang F, Wells G, Anand R, Fletcher S, et al. Comparative pharmacology of epibatidine: a potent agonist for neuronal nicotinic acetylcholine receptors. Mol Pharmacol. 1995; 48:774–82. [PubMed: 7476906]

[31]. Adams DJ, Nutter TJ. Calcium permeability and modulation of nicotinic acetylcholine receptor-channels in rat parasympathetic neurons. J Physiol Paris. 1992; 86:67–76. [PubMed: 1285313]

[32]. Rodrigues-Pinguet NO, Pinguet TJ, Figl A, Lester HA, Cohen BN. Mutations linked to autosomal dominant nocturnal frontal lobe epilepsy affect allosteric Ca^{2+} activation of the α4β2 nicotinic acetylcholine receptor. Mol Pharmacol. 2005; 68:487–501. [PubMed: 15901849]

[33]. Mancias JD, Goldberg J. Structural basis of cargo membrane protein discrimination by the human COPII coat machinery. Embo J. 2008; 27:2918–28. [PubMed: 18843296]

[34]. Wendeler MW, Paccaud JP, Hauri HP. Role of Sec24 isoforms in selective export of membrane proteins from the endoplasmic reticulum. EMBO Rep. 2007; 8:258–64. [PubMed: 17255961]

[35]. Pidoplichko VI, DeBiasi M, Williams JT, Dani JA. Nicotine activates and desensitizes midbrain dopamine neurons. Nature. 1997; 390:401–4. [PubMed: 9389479]

[36]. Wooltorton JR, Pidoplichko VI, Broide RS, Dani JA. Differential desensitization and distribution of nicotinic acetylcholine receptor subtypes in midbrain dopamine areas. J Neurosci. 2003; 23:3176–85. [PubMed: 12716925]

[37]. Heinemann U, Stabel J, Rausche G. Activity-dependent ionic changes and neuronal plasticity in rat hippocampus. Prog Brain Res. 1990; 83:197–214. [PubMed: 2168056]

[38]. Wiest MC, Eagleman DM, King RD, Montague PR. Dendritic spikes and their influence on extracellular calcium signaling. J Neurophysiol. 2000; 83:1329–37. [PubMed: 10712460]

[39]. Mansvelder HD, Keath JR, McGehee DS. Synaptic mechanisms underlie nicotine-induced excitability of brain reward areas. Neuron. 2002; 33:905–19. [PubMed: 11906697]

[40]. Wang H, Sun X. Desensitized nicotinic receptors in brain. Brain Res Brain Res Rev. 2005; 48:420–37. [PubMed: 15914250]

[41]. Lopez-Hernandez GY, Sanchez-Padilla J, Ortiz-Acevedo A, Lizardi-Ortiz J, Salas-Vincenty J, Rojas LV, et al. Nicotine-induced up-regulation and desensitization of α4β2 neuronal nicotinic receptors depend on subunit ratio. J Biol Chem. 2004; 279:38007–15. [PubMed: 15247303]

[42]. Moroni M, Zwart R, Sher E, Cassels BK, Bermudez I. α4β2 nicotinic receptors with high and low acetylcholine sensitivity: pharmacology, stoichiometry, and sensitivity to long-term exposure to nicotine. Mol Pharmacol. 2006; 70:755–68. [PubMed: 16720757]

[43]. Buisson B, Bertrand D. Chronic exposure to nicotine upregulates the human α4β2 nicotinic acetylcholine receptor function. J Neurosci. 2001; 21:1819–29. [PubMed: 11245666]

[44]. Nelson ME, Kuryatov A, Choi CH, Zhou Y, Lindstrom J. Alternate stoichiometries of α4β2 nicotinic acetylcholine receptors. Mol Pharmacol. 2003; 63:332–41. [PubMed: 12527804]

[45]. Buisson B, Gopalakrishnan M, Arneric SP, Sullivan JP, Bertrand D. Human α4β2 neuronal nicotinic acetylcholine receptor in HEK 293 cells: A patch-clamp study. J Neurosci. 1996; 16:7880–91. [PubMed: 8987816]

[46]. Curtis L, Buisson B, Bertrand S, Bertrand D. Potentiation of human α4β2 neuronal nicotinic acetylcholine receptor by estradiol. Mol Pharmacol. 2002; 61:127–35. [PubMed: 11752213]

[47]. Hales TG, Dunlop JI, Deeb TZ, Carland JE, Kelley SP, Lambert JJ, et al. Common determinants of single channel conductance within the large cytoplasmic loop of 5-hydroxytryptamine type 3 and α4β2 nicotinic acetylcholine receptors. J Biol Chem. 2006; 281:8062–71. [PubMed: 16407231]

[48]. Li P, Steinbach JH. The neuronal nicotinic α4β2 receptor has a high maximal probability of being open. Br J Pharmacol. 2010; 160:1906–15. [PubMed: 20649589]

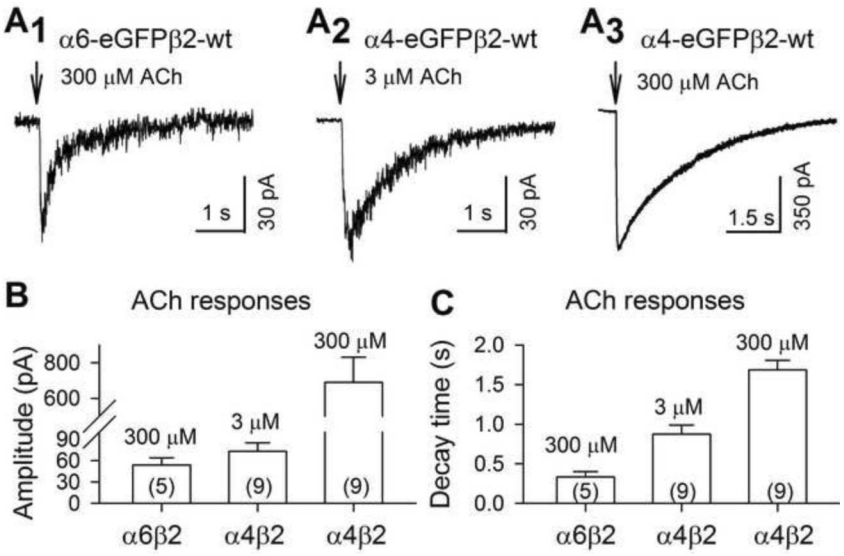

Figure 1.

α6β2 and α4β2 nAChR currents in transfected Neuro-2a cells. (A_{1-3}) Representative traces showing 300 μM ACh-induced current in an α6-eGFPβ2-wt cell (A_1), and 3 μM (A_2) and 300 μM (A_3) ACh-induced currents in an α4-eGFPβ2-wt cell. Arrows indicate 100 ms ACh puffs. Summaries of peak amplitude and decay time constants, respectively, are shown in (B) and (C). Transfected nAChR subunits are indicated on the x-axis. α6β2: α6-eGFPβ2-wt. α4β2: α4-eGFPβ2-wt. ACh concentrations are indicated above each vertical bar (Mean ± SEM). Cell numbers are shown in parentheses.

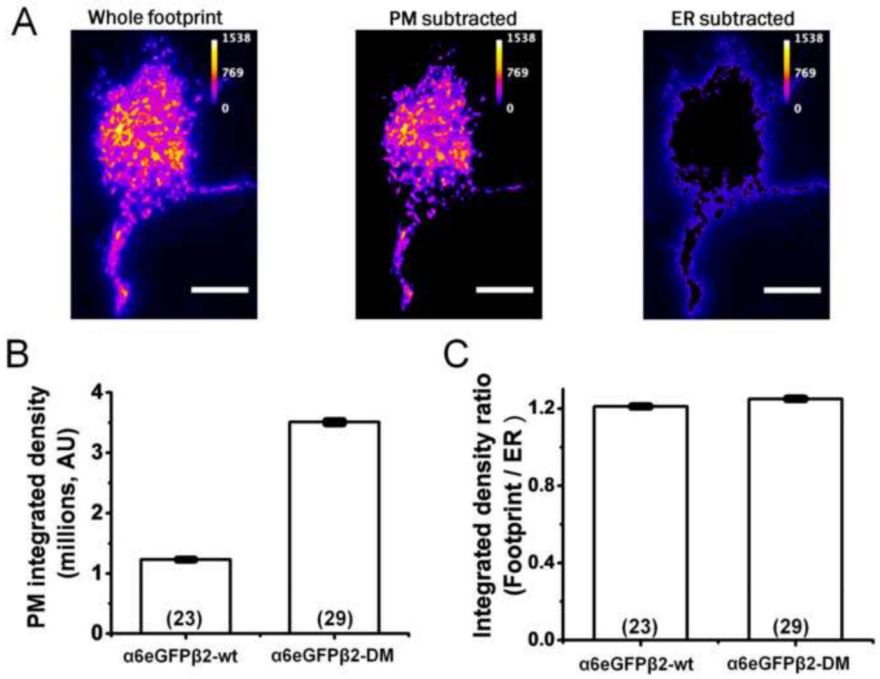

Figure 2.

The β2-DM subunit (also called $\beta2_{\text{enhanced-ER-export}}$) increased fluorescent α6β2 nAChR density in the PM. (A) Representative TIRFM footprint of a Neuro-2a cell expressing α6-eGFPβ2-wt. The TIRF footprint was processed post-acquisition to obtain plasma membrane (PM) subtracted and ER subtracted footprint as indicated. Images are pseudo-colored using the fire-color look up table (LUT), as shown in each panel. Scale bars, 10 μm. (B) Quantification of averaged PM integrated density for TIRF images. Transfected subunits are shown on x-axis. Error bars are 99% confidence interval. (C) Quantification of footprint / ER ratios from TIRF images. Transfected subunits are indicated on x-axis. Error bars are ± 99% confidence limits. Numbers of cells are indicated in parentheses for each graph.

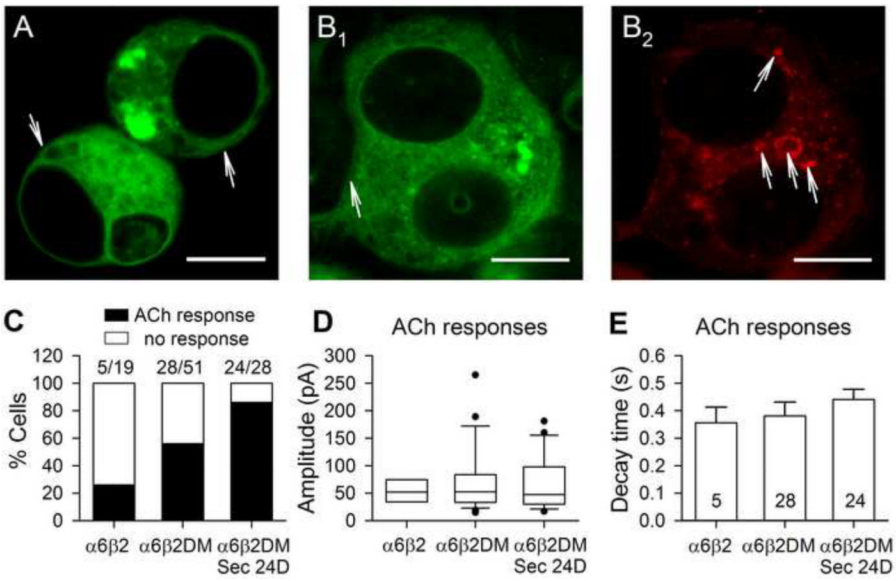

Figure 3.

Improved strategies to detect functional α6β2 nAChRs *in vitro*. (A) Representative images of recorded Neuro-2a cells transfected with α6-eGFPβ2-wt. Arrow: plasma membrane. Scale bar: 10 μm. ($B_{1–2}$) Representative images of a Neuro-2a cell transfected with α6-eGFPβ2-DM plus Sec24D-mCherry, showing α6-eGFP (B_1) and Sec24D-mCherry (B_2). An arrow in (B_1) indicates plasma membrane, which is not well defined. Arrows in (B_2) indicate ER exit sites. Scale bar: 10 μm. (C) Incidences of ACh-induced currents in cells transfected with α6-eGFPβ2-wt, α6-eGFPβ2-DM and α6-eGFPβ2-DM plus Sec24D-mCherry. Black square: % of cells responding to ACh. Gray square: % of cells not responding to ACh. Cell numbers to calculate these percentages are indicated above stacked bars. (D) Box plots of current amplitude in cells transfected with α6-eGFPβ2-wt (n = 5), α6-eGFPβ2-DM (n = 28), or α6-eGFPβ2-DM plus Sec24D-mCherry (n = 24). (E) Summary of decay time constant of 300 μM ACh-induced currents in cells transfected with α6-eGFPβ2-wt, α6-eGFPβ2-DM, and α6-eGFPβ2-DM plus Sec24D-mCherry (Mean ± SEM). Cell numbers are indicated in each vertical bar.

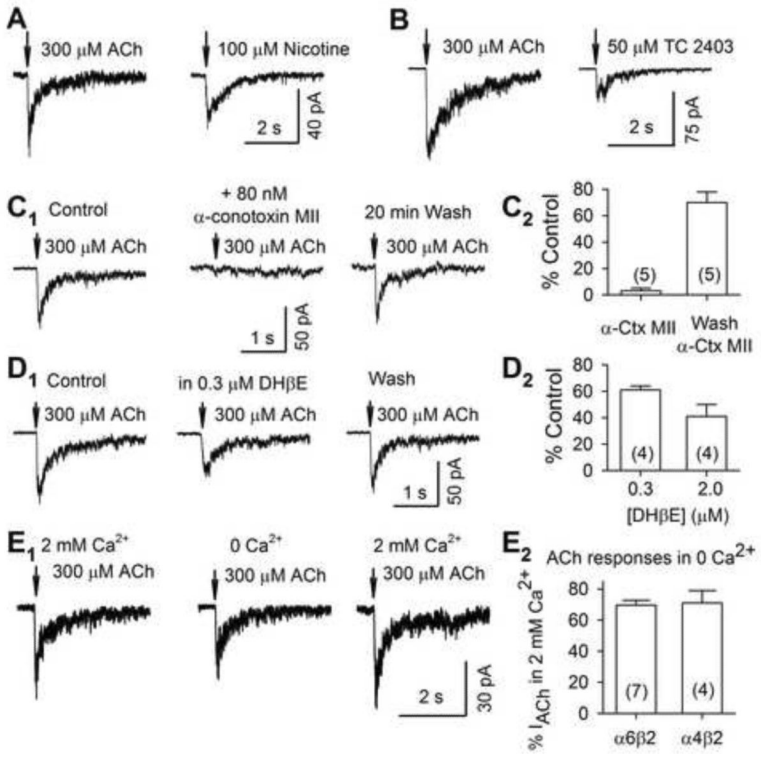

Figure 4.

Pharmacology of α6β2 nAChRs *in vitro*. α6-eGFPβ2-DM nAChRs were activated by either nicotine (A) or TC 2403 (B). ($C_{1–2}$) Typical traces (C_1) and summary (C_2) showing that α6β2 nAChR currents were blocked by 80 nM α-conotoxin MII, and recovered 20 min after washout. ($D_{1–2}$) Typical traces (D_1) and summary (D_2) showing that 0.3 and 2 μM DHβE partially and reversibly inhibited α6-eGFPβ2-DM nAChR currents. ($E_{1–2}$) Both α6-eGFPβ2-DM and α4-eGFPβ2-wt nAChR currents significantly decreased after removal of extracellular Ca^{2+} (0 Ca^{2+}). Cell numbers are shown in parenthesis. Vertical bars show Mean ± SEM. Arrows indicate ACh applications (0.1 s, 20 psi).

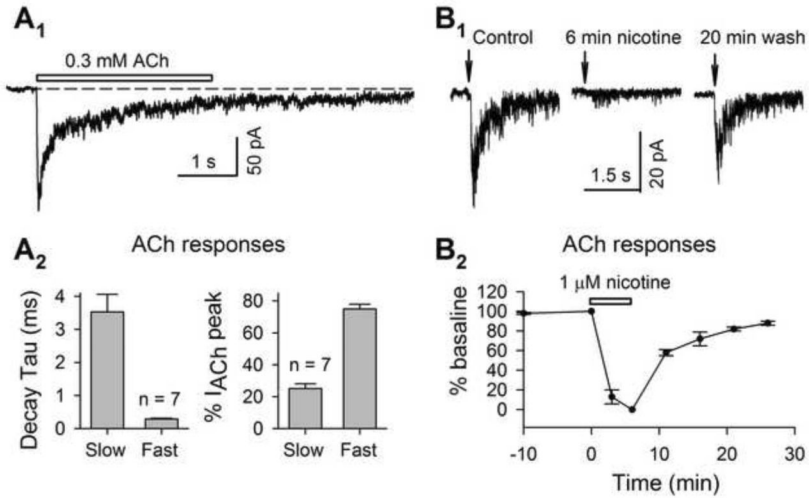

Figure 5.

Desensitization of α6β2 nAChRs *in vitro*. (A_1) A typical trace of 3 s ACh (300 μM) induced α6-eGFPβ2-DM nAChR current. (A_2) The current decay was fitted by two exponential components. The faster component contributed > 70% to the peak amplitude. Cell numbers are indicated in each panel. ($B_{1–2}$) Typical traces (B_1) and summarized time course (B_2, n = 3) showing that α6-eGFPβ2-DM nAChRs desensitized within a few min in 1 μM nicotine, and recovered gradually after nicotine was washed out. Arrows in B_1 indicate ACh applications (0.1 s, 20 psi).

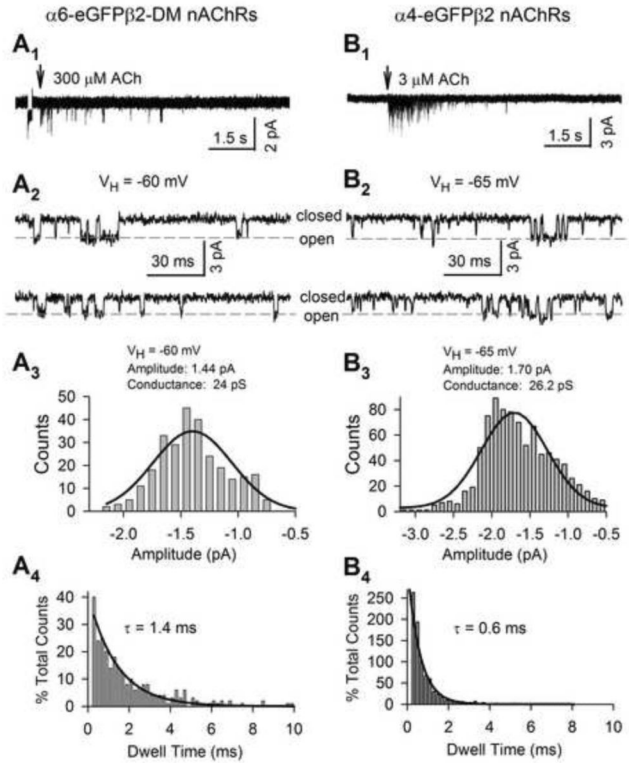

Figure 6.

Single-channel properties of α6β2 and α4β2 nAChRs. A typical trace (8 s) of ACh-induced response in an outside-out patch from a Neuro-2a cell transfected with either α6-eGFPβ2-DM (A_1) or α4-eGFPβ2 (B_1) nAChRs. Arrows indicate ACh applications. An inward current before ACh application in A_1 was caused by a −5 mV voltage step. Typical traces of single level openings of α6-eGFPβ2-DM (induced by 300 μM ACh) and α4-eGFPβ2 nAChRs (induced by 3 μM ACh) are respectively shown in (A_2) and (B_2). Holding potential (V_H), and closed and open states are indicated. Histograms of α6-eGFPβ2-DM and α4-eGFPβ2 nAChR single-channel event amplitude are respectively shown in (A_3) and (B_3). Both were fit to a Gaussian equation (Thick black curve). Histograms of α6-eGFPβ2-DM and α4-eGFPβ2 nAChR single-channel open-time distributions are respectively shown in (A_4) and (B_4). Both were fitted to a single exponential component (Thick black curve). Mean open time (τ) is indicated.